# Role of the Interdomain Linker Probed by Kinetics of CO Ligation to an Endothelial Nitric Oxide Synthase Mutant Lacking the Calmodulin Binding Peptide (Residues 503−517 in Bovine)†

Tomasz Zemojtel,[‡,§,||] Jurgen S. Scheele,[‡,||] Pavel Martásek,[⊥] Bettie Sue Siler Masters,[⊥] Vijay S. Sharma,[@] and Douglas Magde*[,#]

*Departments of Pharmacology I and Medicine I, University of Freiburg, D-79106 Freiburg, Germany, Department of Bioinformatics, University of Wuerzburg, Am Hubland, D-97074 Wuerzburg, Germany, Department of Chemistry and Biochemistry and Department of Medicine, University of California at San Diego, La Jolla, California 92093, and Department of Biochemistry, University of Texas Health Science Center, San Antonio, Texas 78294-7760*

*Received September 20, 2002; Revised Manuscript Received December 20, 2002*

ABSTRACT: Oxygenase and reductase domains in nitric oxide synthase are linked by a peptide region that binds calmodulin. Here we study the effects of modifying the length of the interdomain linker in a deletion mutant lacking 15 amino acids (residues 503−517) in bovine eNOS. The kinetics of CO ligation with the mutant were determined in the presence and absence of tetrahydrobiopterin and arginine and compared with the CO binding kinetics of wild-type eNOS and the eNOS oxygenase domain. In the mutant, electron flow is interrupted. The association kinetics of CO with both mutant and wild-type eNOS can be approximated with two kinetic phases, but the relative proportions change in the mutant. Both the abrogation of electron flow in the mutant and the differences in CO binding may be explained by an alteration in the docking of the FMN domain to the heme domain. We propose that the calmodulin binding residues form a helix that is critical for the proper alignment of the adjacent reductase and oxygenase domains within the active eNOS dimer in achieving proper electron transfer between them.

Members of the nitric oxide synthase (NOS)[1] family of proteins catalyze the conversion of L-arginine to nitric oxide and L-citrulline using NADPH and $O_2$ (*1*). The enzyme is a dimer, each half of which is composed of two distinct domains (*2*−*7*). Each half has an oxygenase domain containing heme along with binding sites for tetrahydrobiopterin ($BH_4$) as a cofactor and L-Arg as a substrate, as well as a reductase domain with binding sites for NADPH, FAD, and FMN (*8*−*10*). These two domains are linked by a peptide region that binds calmodulin (*5*, *7*).

Three isoforms of NOS have been identified. The neuronal (nNOS) and endothelial (eNOS) isoforms are both constitutively expressed and $Ca^{2+}$/calmodulin-dependent, but inducible NOS (iNOS) is immunostimulated at the transcriptional level with CaM binding occurring at such extremely low $Ca^{2+}$ concentrations that it is essentially irreversible (*11*, *12*). All three are homodimers in their physiological states. Recently, evidence has been presented, for iNOS (*13*) and nNOS (*14*), which shows that electron transfer occurs between reductase and oxygenase domains located on adjacent subunits in the dimer. The same is expected to happen in eNOS.

Binding CaM in a $Ca^{2+}$-dependent or -independent manner has been assumed to be a property solely dependent on a canonical CaM binding site involving ∼20−25 amino acids that are highly conserved in NOS. However, chimeric eNOS and nNOS, which have had their CaM binding sequences replaced with the corresponding sequence from iNOS, still required $Ca^{2+}$ for full activity (*12*, *15*).

Deletion of residues 493−512 in eNOS (*12*) resulted in a complete loss of CaM binding capacity and produced a mutant with no capacity to catalyze the conversion of L-Arg to L-citrulline. Further experimental evidence that residues 493−512 in eNOS act as CaM binding regions comes from a study that synthesized modified peptides (*16*) and identified critical amino acids for CaM binding in bovine eNOS: Phe-498, Lys-499, and Leu-511.

It is, however, also possible that the CaM binding peptide, which is immediately adjacent to the N-terminal edge of the FMN binding domain and to the C-terminal end of the heme domain (*17*), may play a role in the proper docking of the reductase domain to the oxygenase domain by maintaining appropriate interdomain orientations. Such a role has been demonstrated in another protein that shares with NOS a similar domain organization, cytochrome P450 BM-3 (*18*, *19*). In that case, it was found that the length of the peptide (residues 460−475 in *Bacillus megaterium*) linking the FMN

† This work was supported in part by National Institutes of Health Grants HL30050 and GM52419 (to B.S.S.M.) and Grant AQ-1192 from the Robert A. Welch Foundation (to B.S.S.M.).

* To whom correspondence should be addressed. E-mail: dmagde@ucsd.edu. Fax: (858) 534-0130. Phone: (858) 534-3199.

‡ University of Freiburg.

§ University of Wuerzburg.

|| These authors contributed equally to this work.

⊥ University of Texas Health Science Center.

@ Department of Medicine, University of California at San Diego.

# Department of Chemistry and Biochemistry, University of California at San Diego.

[1] Abbreviations: NOS, nitric oxide synthase(s); eNOS, endothelial NOS; nNOS, neuronal nitric oxide synthase; iNOS, inducible nitric oxide synthase; $BH_4$, tetrahydrobiopterin; WT, wild type.

10.1021/bi026886w CCC: $25.00 © 2003 American Chemical Society
Published on Web 05/08/2003

```
                    Δ
ENOS_BOVINE 498 FKEVANAVKISASLMGTLMAKRVKAT 523
                *::. .   *.*   :    * **
CP450-BM3_BM 450 SKKIPLGGIPSPSTEQSAKKVRKKAE 475
```

FIGURE 1: Alignment of the sequence of peptides linking FMN and oxygenase domains in eNOS (bovine) and in cytochrome P450 BM-3 (*B. megaterium*), with the truncated region (residues 503−517 in bovine eNOS) noted, as obtained using ClustalX (version 1.81).

and oxygenase domains is critical for correctly orienting the reductase and heme domains and in achieving efficient electron transfer from the FMN domain to the heme domain. Interestingly, a best local sequence alignment reveals that P450 BM-3 and eNOS are homologous in this region (Figure 1). It is also noteworthy that two of three residues that are important for CaM binding (Phe-498 and Leu-511 in eNOS) are not present in P450 BM-3 and that the latter enzyme does not bind CaM *in vivo*.

All this motivated us to prepare an eNOS protein mutant lacking 15 amino acids in the calmodulin binding region (residues 503−517 in bovine) (Figure 1).

We have previously shown in the nNOS−CO system (*20*), that the kinetics of rebinding of CO are sensitive to the presence or absence of the reductase domains. Therefore, it is a plausible hypothesis that CO kinetics should prove to be sensitive to any alteration in the relative positions of the oxygenase and reductase domains, as they are likely to be introduced by truncation of the interdomain linker. To assess this hypothesis, we compared the eNOS (residues 503−517) mutant's bimolecular CO binding kinetics, associated with ligand entry from the solvent into the heme pocket, with kinetics in the wild-type protein and in the heme domain fragment.

## MATERIALS AND METHODS

The heme domain of bovine WT-eNOS (eNOS HD) was prepared as follows. We first purified bovine holo WT-eNOS as described previously (*21*). The peak fractions consisting of the dimeric form were collected. Subsequent trypsinolysis (*22*) yielded HD in the same amounts and purity as described previously (*23*). HD was purified using a sizing column, and the peak dimeric fractions were used in the study.

A variant of bovine holo WT-eNOS missing 15 amino acids (residues 503−517) in its calmodulin (CaM) binding region and designated as Δ(503−517) eNOS was obtained as follows. Bovine WT-eNOS cDNA in the pCWori+ vector was digested by *Bal*I (two restriction sites encompass the sequence for CaM binding), gel-purified, and religated. This led to in-frame deletion of eNOS amino acids 503−517 from the CaM binding area. Then the Δ(503−517) eNOS variant protein was purified in the manner described previously for the purification of bovine WT-eNOS (*21*).

Carbon monoxide (99.8%), high-purity argon, and mixtures of CO (1−100%) diluted in argon were from Matheson. Buffers [20 mM Tris-HCl (pH 7.8), 100 mM EDTA, and 100 mM NaCl] were prepared in a septum-sealed 10 mm fused silica optical cell (Hellma QS 105.250) and deoxygenated by bubbling with argon for 40 min. Then, CO or a CO/Ar mixture was bubbled through the cell for at least 10 min. When indicated, buffers contained 250 μM $BH_4$ and/or 10 mM L-Arg. Meanwhile, deoxygenated protein solutions were reduced using 1 part in 50 of a 1% sodium dithionite solution degassed with argon. Last, protein was added to cells prepared with the desired ligand concentration. The final concentration of the protein samples was ∼2 μM.

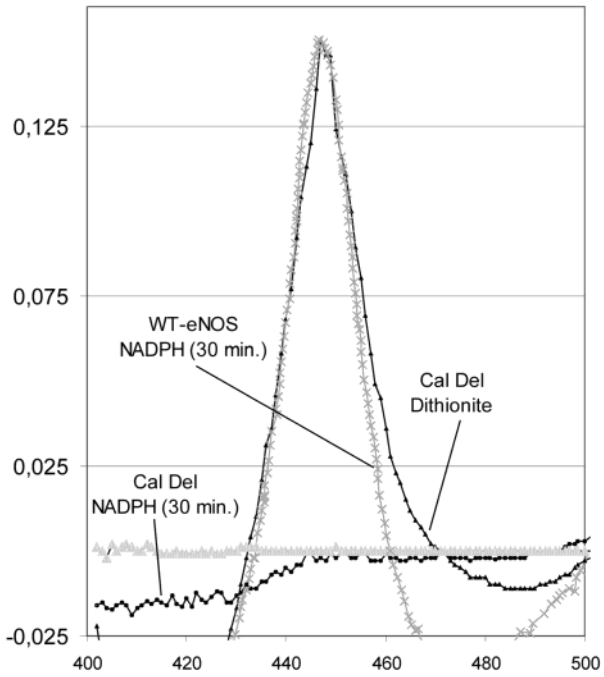


FIGURE 2: UV−visible spectra of Δ(503−517) eNOS (Cal Del) in buffer containing L-Arg and $BH_4$ and saturated with CO alone or with additives as noted. Spectra of NADPH-reduced WT-eNOS (L-Arg and $BH_4$ repleted) have been added for comparison.

Flash photolysis was carried out at 22 °C using procedures described previously (*20*, *24*). Kinetics were monitored at several wavelengths showing both transient absorption and initial state bleaching. Transients for kinetic analyses were recorded mostly at 445 or 420 nm.

## RESULTS

The Δ(503−517) eNOS mutant protein was first tested for its ability to bind CaM. The mutant exhibited a sharply diminished binding affinity for CaM, as will be described in detail elsewhere. We should note that calmodulin binding experiments show that other sites are also important in binding. Deletion of residues 493−513 of eNOS results in the complete loss of CaM binding (*16*), so those other sites could well be located within residues 493−502 of eNOS.

Next we tested whether reduction of the heme iron with NADPH could still occur in the mutant by electron transfer from the reductase domain. The NADPH concentration was varied over a range of [NADPH]/[heme] ratios from 10 to 30. As judged by UV−visible spectra, reduction does not occur. Data are shown in Figure 2 for spectra recorded in the presence of L-Arg and $BH_4$ monitored over the course of 30 min. The same result was obtained even for much longer incubation times. The results were the same in the absence of L-Arg and $BH_4$. Addition of dithionite, however, did reduce the heme as manifested by the appearance of a characteristic band centered around 445 nm. So it seems clear that electron transfer was blocked in the mutant. We verified that under the same protocol NADPH-mediated reduction of the heme iron was observed for WT-eNOS (Figure 2).

```
PSIpred: Code: H=Helix, C=Coil, E=Strand
            620216998989999999999887515782
               CCEECHHHHHHHHHHHHHHHHHHCCCCC
         493 TRKKTFKEVANAVKISASLMGTLMAKRVK 521

PHD:      Code: H=Helix
            654169999999999999999999423
                HHHHHHHHHHHHHHHHHHHHHHH
         493 TRKKTFKEVANAVKISASLMGTLMAKRVK 521

SSpro2:  Code: H=Helix, E=Strand, C=Other

               CCCHHHHHHHHHHHHHHHHHHHHHHCCE
         493 TRKKTFKEVANAVKISASLMGTLMAKRVK 521
```

FIGURE 3: Three secondary structure-predicting programs all agree that residues 503−517 should be part of an α-helix. For the top two programs, the numbers above the predictions are levels of confidence (9 being the highest) supplied by the programs.

*The Region Deleted*. The peptide region of residues 503−517 in eNOS (bovine) is certainly involved in the interface between the reductase and oxygenase domains. It is thought to be part of an α-helix. Since a helical segment would be likely to enforce a rather well-defined relation between domains, its deletion should have consequences for domain orientations. To provide some specific justification for this starting point, it is useful to see what secondary structure might be predicted for the fragment by structure-predicting computer software. We analyzed the amino acid sequence of the deleted peptide using three different secondary structure prediction programs, namely, PSIpred (*25*, *26*), PHD (*25*, *26*), and SSpro2 (*27*, *28*). All three agreed that there is a high probability of a helical conformation. In Figure 3, we display the three predictions.

With those matters settled, we explored the question of whether the Δ(503−517) deletion has any effect on the kinetics of ligation at the iron binding site.

*Association Kinetics of Carbon Monoxide.* After flash photolysis of an Fe−CO bond, some amount of CO escapes into the solvent, leaving behind reactive iron sites ready to bond to CO. Over the micro- to millisecond time range, a CO molecule from the reservoir of excess CO in the solvent re-enters the protein, moves as necessary through the protein matrix, and ultimately binds to the heme iron.

The kinetics of CO binding were characterized for three species: (1) the Δ(503−517) eNOS mutant of interest, (2) the wild-type eNOS holoenzyme, and (3) the heme domain of eNOS. We used three or four different sample preparations of each and found results to be highly reproducible. For each species, data were collected under four conditions: (N) in the absence of both L-Arg and $BH_4$, (A) in the presence of L-Arg but not $BH_4$, (B) in the presence of $BH_4$ but not L-Arg, and (A&B) in the presence of both L-Arg and $BH_4$. For each of the three protein species and for any combination of L-Arg and $BH_4$, flash photolysis led to transient absorbance changes in the visible spectral region that were consistent with the dissociation of CO from the protein followed by return of CO from the surrounding solution to the heme. The reaction is highly reversible; hundreds of photolyses produce no permanent changes. That this represented a bimolecular association reaction was proven by repeating the measurement with different concentrations of CO in the solution. The observed reaction course became faster at higher CO concentrations. In no case could the bimolecular combination be interpreted as a single-exponential process. Absorbance changes had to be fit to a sum of two exponential terms, named here the fast and slow phases. The characteristic rates for the two processes obtained from the best fits were plotted separately versus CO concentration to obtain the second-order, bimolecular rate constants for the fast and slow processes discussed below. The rate constants are displayed in Table 1.

Table 1: Rate Constants for CO Binding to the eNOS Holoenzyme, Deletion Mutant, and Heme Domain

| system | $k_f$ ($mM^{-1}$ $s^{-1}$) | $k_s$ ($mM^{-1}$ $s^{-1}$) |
|---|---|---|
| holo | 800 ± 15 | 6.5 ± 0.4 |
| holo and A | 170 ± 15 | 6.5 ± 0.5 |
| holo and B | 830 ± 15 | 7.0 ± 0.5 |
| holo, A, and B | 120 ± 10 | 7.5 ± 0.6 |
| Δ(503−517) | 1170 ± 30 | 6.5 ± 0.5 |
| Δ(503−517) and A | 170 ± 10 | 6.5 ± 0.5 |
| Δ(503−517) and B | 1250 ± 25 | 7.5 ± 0.4 |
| Δ(503−517), A, and B | 130 ± 10 | 7.5 ± 0.5 |
| Hm Dm | 1150 ± 10 | 5.8 ± 0.4 |
| Hm Dm and A | 1100 ± 10 | 5.3 ± 0.3 |
| Hm Dm and B | 1200 ± 15 | 6.1 ± 0.4 |
| Hm Dm, A, and B | 1230 ± 20 | 5.6 ± 0.3 |

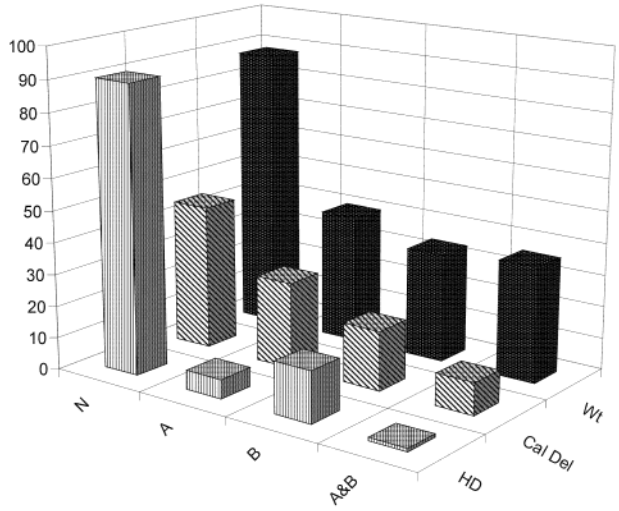


FIGURE 4: Percentage of amplitude in the fast phase for CO association with various eNOS preparations: results for the heme domain (HD) of the WT enzyme (front row), Δ(503−517) eNOS (Cal Del) (middle row), and WT holoenzyme (Wt) (back row). Along each row, data labeled N have neither $BH_4$ nor L-Arg, A have 10 mM L-Arg, B have 250 μM $BH_4$, and A&B have both.

Under the different (N, A, B, or A&B) buffer conditions for each protein, there were sizable differences in the fractional amounts of the fast and slow components. A pictorial representation of the fraction contributed by the fast phase appears in Figure 4. In all cases, the rate constant describing the slow phase remained near 7 $mM^{-1}$ $s^{-1}$. The fast rate changed. The ratio of fast to slow rate constants, $k_f/k_s$, in different preparations ranged from 16 to 203.

## DISCUSSION

The most important inference we draw from the CO kinetic studies depends simply on the fact that there are substantial differences in behavior in the Δ(503−517) mutant and WT-eNOS enzyme and the eNOS oxygenase domain. Exactly how structural features correlate with kinetic rate constants is a very difficult question, the answer to which is beyond the current state of the art even for proteins that are simpler

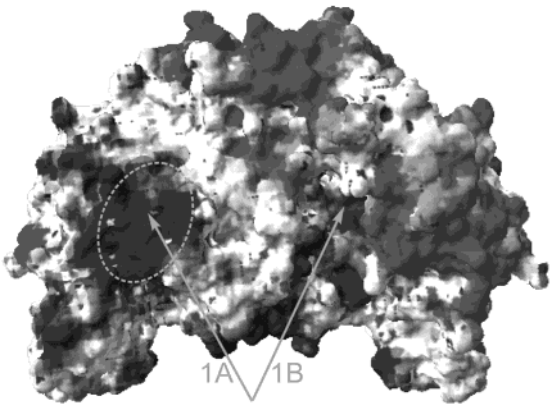


FIGURE 5: Electrostatic potential mapped onto the surface of the eNOS heme domain dimer (PDB entry 4NSE). The calculation was performed using Swiss PDB viewer 3.7 (b2) (dielectric constant of the protein = 4.00, dielectric constant of the solvent = 80.00, employed in Poisson−Boltzmann calculations). Positively charged regions are darker, and negatively charged regions are lighter. Arrows mark entry channels (1A and 1B) to the heme pocket. A dashed ellipse marks region of positive electrostatic potential surrounding the exposed edge of heme, a possible FMN docking site.

and have been studied far longer than the NOS family has been. As explained above, all systems exhibited CO combination comprised of two phases, one termed fast and the other slow, with the feature of interest being the relative proportions of the two phases.

*The Reductase Domain Inhibits Kinetic Rates*. The fact that CO binding kinetics are different for the heme domain and for WT-eNOS implies some influence of the reductase domain on the distribution of amplitudes of the fast and slow phases in WT-eNOS. That in turn suggests that changes at the domain interface, as are likely to be induced in the Δ-(503−517) deletion mutant, might well be reflected in CO binding.

A recently reported structure (*29*) for the complex between the heme and FMN binding domains in a structurally related heme protein, cytochrome P450 BM-3, reveals "cross talk" at the docking interface involving methyl groups of FMN positioned toward the heme binding loop. Taking into account the homology in reductase domains of P450 and NOS and a similarity in the structures of their heme binding loops (*30*), one may expect a like interaction in NOS proteins. Figure 5 depicts a possible FMN docking site. A recent paper offers further support for this analogy by describing an electron transfer-active chimera composed of the oxygenase domain of nNOS and the reductase domain of P450 BM-3 (*31*).

The three known members of the NOS family, despite many similarities, differ profoundly from each other. It is immediately clear that iNOS differs in its function and in the role that CaM and $Ca^{2+}$ play; however, eNOS and nNOS also differ from each other, particularly in activity at their iron centers, while nNOS is more similar to iNOS in some behaviors. A totally different effect of the reductase domain on CO binding in the oxygenase domain is observed when one compares eNOS and nNOS. In our earlier CO photolysis experiments with nNOS (*22*), for the nNOS heme domain by itself, the fraction of fast phase was scarcely sensitive to either L-Arg or $BH_4$ alone, although in combination there was an effect. For the full-length enzyme, the presence of the nNOS reductase domain made a substantial change in CO binding kinetics, converting what was essentially a fast reacting oxygenase domain into a holoenzyme system in which the amplitude of the slow phase was around 90%. In eNOS, we saw an opposite effect; that is, the oxygenase domain exhibited CO binding kinetics dominated by the slow phase, whereas the intact WT-eNOS with the reductase domain present produced kinetics with comparable fractions in each phase (Figure 4). Another dramatic difference is that eNOS exhibits heme reduction that is 10 thousand times slower than in nNOS: $5 \times 10^{-4}$ $s^{-1}$ for eNOS compared to 4 $s^{-1}$ for nNOS (*32*). Experiments with chimeras comprised of swapped oxygenase and reductase domains of nNOS and eNOS (*33*, *34*) show that the reductase domain of eNOS contains structural elements that are distinct from those in iNOS and nNOS. The eNOS investigations reported here revealed that eNOS does exhibit geminate recombination on the nanosecond time scale, as did nNOS (*22*); however, that behavior shed no light on the issues addressed herein, and we do not wish to speculate about the implications of geminate rebinding until we can treat the behavior on all time scales from sub-picosecond to microsecond. Since the various NOS forms do differ, and since we think it is premature to try to compare them, we believe the appropriate thing to do is to try to work within the framework of an already published model for eNOS.

*Heterogeneity of Heme Centers Probed by Binding of CO to WT-eNOS*. We tested the applicability of a model advanced by Berka et al. (*35*), who proposed that the two heme centers in the eNOS dimer may be functionally distinct and exhibit different ligand binding kinetics. The heterogeneity they report was observed while NO binding to eNOS with L-Arg bound was being investigated. Since CO shows a richer binding behavior than NO does, it is of interest to test whether their conjecture can offer a plausible interpretation of CO ligation kinetics.

The general effect of adding L-Arg or $BH_4$ to any of our eNOS preparations is, according to Figure 4, a decrease in the amplitude of the fast phase and an increase in the amount of slow phase, in effect, a conversion of fast to slow. In WT-eNOS, the (N) case exhibits predominately fast kinetics, while for the (A), (B), and (A&B) cases, something approaching, but definitely less than, 50% of the amplitude appears in the slow phase. Since there is already some slow phase even for the (N) condition, one might interpret that small percentage (∼10%) of slow phase under the (N) condition as a "background" level, which should be ignored in calculating what fraction of the fast phase process is converted to slow for each circumstance. We might then divide the increase in slow amplitude by the (N)-state fast fractional amplitude to obtain a conversion percentage. The result for WT-eNOS is shown in Figure 6. With this estimate, slightly more than 50% of the fast phase is converted to the slow phase. While hardly compelling proof of the model of Berka et al. (*35*), our data are consistent with their model, which would assign the fast phase to one heme center and the slow phase to the second heme center in the eNOS dimer.

Another argument in favor of the two heme centers being distinct in eNOS comes from the observation that in the absence of substrate approximately half of the heme in eNOS is reduced by excess NADPH (*32*) while in the same environment iNOS and nNOS are fully reduced (*36*).

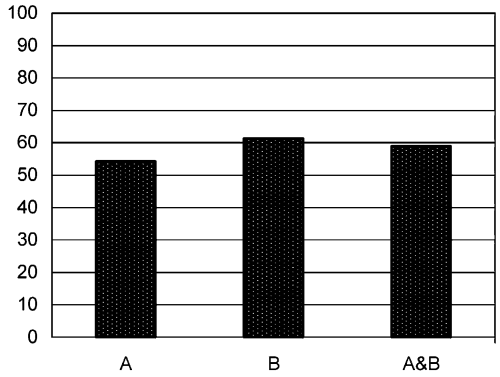


FIGURE 6: Percentage of fast phase CO combination in WT-eNOS that is converted to slow phase by L-Arg and $BH_4$ after correction for a background component, as discussed in the text.

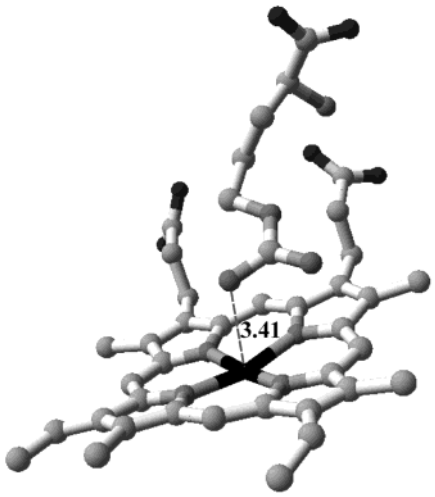


FIGURE 7: Ferrous human eNOS with L-Arg (PDB entry 1FOL). Modeled with Swiss PDB viewer 3.7 (b2). The dashed line marks a distance from the guanidino nitrogen, NH1, of L-Arg to the heme iron: 0.341 nm in one heme center and 0.389 nm in the second. In the ferric form (PDB entry 4NSE), the distances are longer: 0.377 nm in one heme center and 0.436 nm in the other.

One expects that changes in the kinetics of ligand binding to the holoenzyme should depend primarily on effects localized in the oxygenase domain. The crystal structure of the full NOS unit, composed of docked oxygenase and reductase domains, has not been determined yet, but the crystal structure of the eNOS oxygenase (heme) domain reveals heme located on a side of the heme domain (*22*, *37*, *38*), as marked by arrow 1A in Figure 5. It also shows L-Arg sitting directly above the heme iron, as in Figure 7 (*22*, *37*, *38*).

Our analyses of the eNOS crystal structures of the L-Arg-bound oxygenase domain (*37*) reveal small, but possibly significant, differences between the two heme centers with respect to distances from the guanidino nitrogen, NH1, of L-Arg to the heme iron (0.59 Å of the difference in the oxidized form and 0.48 Å in the reduced form) (Figure 7). In iNOS, these differences are smaller, less than 0.2 Å (PDB entry 1NSI). If docking of the FMN domain involves, as in the P450 BM-3 case, interaction with a heme binding loop, that could be translated into a longer distance between the iron in the heme plane and the substrate in the oxygenase domain of eNOS, resulting in one CO binding site with diminished sensitivity to the presence of a substrate and/or cofactor. With this background, we turn to the behavior of the truncated species.

*The heme domain (oxygenase domain)*, by itself, exhibits CO binding that can be described by a combination of fast and slow phases, as needed for the holoenzyme. However, almost all the amplitude is converted to the slow phase when either L-Arg or $BH_4$ is bound, providing no evidence at all for two distinguishable sites. In particular, the extremely low percentage (~1%) of fast phase when L-Arg and $BH_4$ are both bound, as seen in Figure 4, shows that, when applying the Berka model, both CO binding sites are sensitive to substrate, suggesting that L-Arg binding is enhanced by $BH_4$ (*39*). Furthermore, what small amount of fast phase persists under the different conditions in Figure 4 shows a very fast rate constant in all cases (Table 1).

*Possible Conformational Changes in the Δ(503−517) eNOS Mutant.* Our computer analyses of secondary structure showed that that the deleted peptide is probably helical in conformation. Other work (*40*) also suggests that the peptide sequences recognized by CaM and $Ca^{2+}$ are probably helical while part of an intact protein. Truncation of this region should not alter the structural conformations of the N-terminal edge of the FMN binding domain and the C-terminal edge of the heme domain to which it is immediately adjacent (*17*). Therefore, any alteration in positioning of the reductase domain, such as removing a helix linking it with the oxygenase domain, is translated into a change in the relative positions of and distances between the two domains. This in turn should influence the gating of ligand entry into the two heme centers. Two possible gating channels present on both sides of the dimer are marked in Figure 5.

The notion that the FMN domain in the mutant is precluded from docking at its native site is supported by the inability of NADPH to reduce the Δ(503−517) eNOS mutant's iron to $Fe^{2+}$ (demonstrated in Figure 2). This is a result of stopping electron flow from the FMN domain to the heme iron. A schematic visualization is shown in Figure 8B. Moreover, it has been shown for a protein with a similar domain organization, cytochrome P450 BM-3, that the length of the linker is important for correctly orienting the reductase and heme domains for electron transfer (*18*, *19*).

Figure 4 shows that the Δ(503−517) mutant behaves in a way that is intermediate between those of WT-eNOS and the isolated, but dimeric, heme domain, consistent with a disturbance close to the heme iron and part of the way toward removal of the reductase domain altogether. The situation can be reconciled with the Berka model. It is, however, premature to claim real validation for that model or any other, or to speculate about details. Analysis of CO binding kinetics in both the Δ(503−517) mutant and WT-eNOS involves complicated proteins, in which the reductase domain docks to an oxygenase domain located on an adjacent subunit in the dimer. We do not have a crystal structure for anything but one domain; we do not know much about how docking is altered in the mutant, and we do not know how that is translated into effects on kinetic rates. Currently, in our laboratory, we are trying to define pathways for ligand entry into the heme pocket by *in silico* modeling techniques and planning to study ligand kinetics on the nano- and picosecond time scales, which probe more specifically the heme environment than do kinetic studies of the overall binding process.

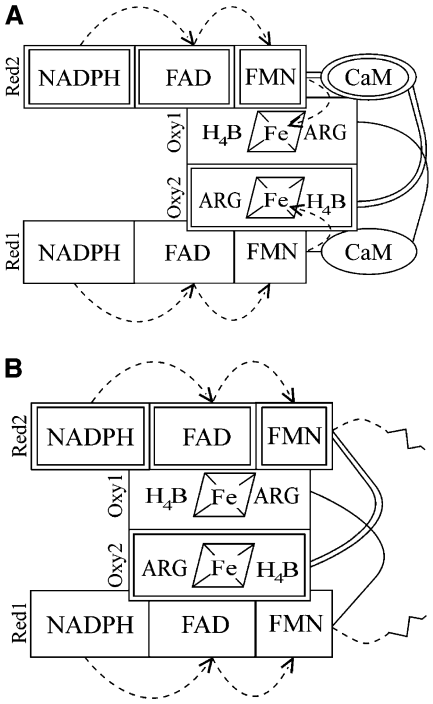


FIGURE 8: Scheme for hypothesized interdomain electron transfer mediated by NADPH and the disruption caused by the Δ(503−517) deletion: (A) WT-eNOS and (B) Δ(503−517) eNOS. Red1 and Red2 are reductase domains of subunits 1 and 2, respectively. Oxy1 and Oxy2 are oxygenase domains of subunits 1 and 2, respectively. Dashed arrows illustrate the interdomain electron flow pathway. In the absence of direct evidence, but with the need to make some assumption to draw the figure, electron transfer is shown occurring between the reductase and oxygenase domains located on different subunits of the dimer as proposed by Stuehr et al. for iNOS (*13*) and nNOS (*14*).

*Summary.* Our results clearly show an influence on the distribution of amplitudes of the kinetic phases in eNOS ligation due to the presence of the reductase domain or to an alteration in its docking geometry. Removing residues 503−517 of the peptide linking the two domains leads to a change in the relative orientation of the reductase domain and the oxygenase domain. Such an alteration in the position of the reductase domain might influence ligand binding kinetics either by creating or blocking "channels" that lead from the solution to the heme centers or by causing conformational changes in the vicinity of the heme binding loop. Thus, residues 503−517 in eNOS not only play an essential role in calmodulin binding but also are involved in maintaining correct docking of the FMN domain to the oxygenase domain for proper electron transfer between them. Figure 8 attempts to convey a sense of what we believe is involved.

## ACKNOWLEDGMENT

We thank reviewers for helpful suggestions. D.M. thanks the late Prof. K. Wilson.

## REFERENCES

1. Bredt, D. S., and Snyder, S. H. (1990) *Proc. Natl. Acad. Sci. U.S.A. 87*, 682−685.
2. Sheta, E. A., McMillan, K., and Masters, B. S. (1994) *J. Biol. Chem. 269*, 15147−15153.
3. McMillan, K., Bredt, D. S., Hirsch, D. J., Snyder, S. H., Clark, J. E., and Masters, B. S. (1992) *Proc. Natl. Acad. Sci. U.S.A. 89*, 11141−11145.
4. Forstermann, U., Schmidt, H. H., Pollock, J. S., Sheng, H., Mitchell, J. A., Warner, T. D., Nakane, M., and Murad, F. (1991) *Biochem. Pharmacol. 42*, 1849−1857.
5. Pollock, J. S., Forstermann, U., Mitchell, J. A., Warner, T. D., Schmidt, H. H., Nakane, M., and Murad, F. (1991) *Proc. Natl. Acad. Sci. U.S.A. 88*, 10480−10484.
6. Bredt, D. S., Hwang, P. M., Glatt, C. E., Lowenstein, C., Reed, R. R., and Snyder, S. H. (1991) *Nature 351*, 714−718.
7. Xie, Q. W., Cho, H. J., Calaycay, J., Mumford, R. A., Swiderek, K. M., Lee, T. D., Ding, A., Troso, T., and Nathan, C. (1992) *Science 256*, 225−228.
8. Chen, P. F., Tsai, A. L., Berka, V., and Wu, K. K. (1996) *J. Biol. Chem. 271*, 14631−14635.
9. Ghosh, D. K., and Stuehr, D. J. (1995) *Biochemistry 34*, 801−807.
10. McMillan, K., and Masters, B. S. (1995) *Biochemistry 34*, 3686−3693.
11. Cho, H. J., Xie, Q. W., Calaycay, J., Mumford, R. A., Swiderek, K. M., Lee, T. D., and Nathan, C. (1992) *J. Exp. Med. 176*, 599−604.
12. Venema, R. C., Sayegh, H. S., Arnal, J. F., and Harrison, D. G. (1995) *J. Biol. Chem. 270*, 14705−14711.
13. Siddhanta, U., Presta, A., Fan, B., Wolan, D., Rousseau, D. L., and Stuehr, D. J. (1998) *J. Biol. Chem. 273*, 18950−18958.
14. Panda, K., Ghosh, S., and Stuehr, D. J. (2001) *J. Biol. Chem. 276*, 23349−23356.
15. Ruan, J., Xie, Q., Hutchinson, N., Cho, H., Wolfe, G. C., and Nathan, C. (1996) *J. Biol. Chem. 271*, 22679−22686.
16. Venema, R. C., Sayegh, H. S., Kent, J. D., and Harrison, D. G. (1996) *J. Biol. Chem. 271*, 6435−6440.
17. Salerno, J. C., Harris, D. E., Irizarry, K., Patel, B., Morales, A. J., Smith, S. M., Martasek, P., Roman, L. J., Masters, B. S., Jones, C. L., Weissman, B. A., Lane, P., Liu, Q., and Gross, S. S. (1997) *J. Biol. Chem. 272*, 29769−29777.
18. Govindaraj, S., and Poulos, T. L. (1995) *Biochemistry 34*, 11221−11226.
19. Govindaraj, S., and Poulos, T. L. (1996) *Protein Sci. 5*, 1389−1393.
20. Scheele, J. S., Kharitonov, V. G., Martasek, P., Roman, L. J., Sharma, V. S., Masters, B. S., and Magde, D. (1997) *J. Biol. Chem. 272*, 12523−12528.
21. Martasek, P., Liu, Q., Liu, J., Roman, L. J., Gross, S. S., Sessa, W. C., and Masters, B. S. (1996) *Biochem. Biophys. Res. Commun. 219*, 359−365.
22. Raman, C. S., Li, H., Martasek, P., Kral, V., Masters, B. S., and Poulos, T. L. (1998) *Cell 95*, 939−950.
23. Zhang, J., Martasek, P., Paschke, R., Shea, T., Siler Masters, B. S., and Kim, J. J. (2001) *J. Biol. Chem. 276*, 37506−37513.
24. Scheele, J. S., Bruner, E., Kharitonov, V. G., Martasek, P., Roman, L. J., Masters, B. S., Sharma, V. S., and Magde, D. (1999) *J. Biol. Chem. 274*, 13105−13110.
25. Rost, B., and Sander, C. (1993) *J. Mol. Biol. 232*, 584−599.
26. Rost, B., and Sander, C. (1994) *Proteins 19*, 55−72.
27. Baldi, P., Brunak, S., Frasconi, P., Soda, G., and Pollastri, G. (1999) *Bioinformatics 15*, 937−946.
28. Pollastri, G., Baldi, P., Fariselli, P., and Casadio, R. (2001) *Bioinformatics 17* (Suppl. 1), S234−S242.
29. Sevrioukova, I. F., Li, H., Zhang, H., Peterson, J. A., and Poulos, T. L. (1999) *Proc. Natl. Acad. Sci. U.S.A. 96*, 1863−1868.
30. Crane, B. R., Arvai, A. S., Gachhui, R., Wu, C., Ghosh, D. K., Getzoff, E. D., Stuehr, D. J., and Tainer, J. A. (1997) *Science 278*, 425−431.
31. Fuziwara, S., Sagami, I., Rozhkova, E., Craig, D., Noble, M. A., Muro, A. W., Chapman, S. K., and Shimizu, T. (2002) *J. Inorg. Biochem. 91*, 515−526.
32. Abu-Soud, H. M., Ichimori, K., Presta, A., and Stuehr, D. J. (2000) *J. Biol. Chem. 275*, 17349−17357.
33. Nishida, C. R., and Ortiz de Montellano, P. R. (1998) *J. Biol. Chem. 273*, 5566−5571.
34. Adak, S., Aulak, K. S., and Stuehr, D. J. (2001) *J. Biol. Chem. 276*, 23246−23252.
35. Berka, V., and Tsai, A. L. (2000) *Biochemistry 39*, 9373−9383.
36. Abu-Soud, H. M., and Stuehr, D. J. (1993) *Proc. Natl. Acad. Sci. U.S.A. 90*, 10769−10772.

37. Li, H., Raman, C. S., Martasek, P., Masters, B. S., and Poulos, T. L. (2001) *Biochemistry 40*, 5399−5406.
38. Fischmann, T. O., Hruza, A., Niu, X. D., Fossetta, J. D., Lunn, C. A., Dolphin, E., Prongay, A. J., Reichert, P., Lundell, D. J., Narula, S. K., and Weber, P. C. (1999) *Nat. Struct. Biol. 6*, 233−242.
39. Klatt, P., Schmid, M., Leopold, E., Schmidt, K., Werner, E. R., and Mayer, B. (1994) *J. Biol. Chem. 269*, 13861−13866.
40. Brokx, R. D., Lopez, M. M., Vogel, H. J., and Makhatadze, G. I. (2001) *J. Biol. Chem. 276*, 14083−14091.

BI026886W